

Collisional- and photo-excitations of Ca IV including strong $3.2 \mu\text{m}$ emission line

Sultana Nahar^{1*} and Bilal Shafique^{2†}

^{1*}Astronomy Department, The Ohio State University, 140 W.
18th Ave, Columbus, 43210 , OH , USA .

²Physics Department, University of Azad Jammu and Kashmir, ,
Muzzafarabad, 13100, Kashmir , Pakistan.

*Corresponding author(s). E-mail(s): nahar.1@osu.edu;

Contributing authors: bilalshafiquehawaja@ajku.edu.pk;

†These authors contributed equally to this work.

Abstract

We report a detailed study of features of electron-impact excitation (EIE) of Ca IV ($\text{Ca IV} + e \rightarrow \text{Ca IV}^* + e' \rightarrow \text{Ca IV} + h\nu + e'$), for the first time using the relativistic Breit-Pauli R-Matrix method with a large close coupling wavefunction expansion of 54 fine structure levels belonging to $n=2,3,4$ complexes. Calcium lines in the infrared (IR) are expected to be observed by the high resolution James Webb Space Telescope. Our study predicts presence of a strong $3.2 \mu\text{m}$ emission line in IR formed due to EIE of $3p^5 \ ^2P_{3/2}^o - 3p^5 \ ^2P_{1/2}^o$ in Ca IV. The EIE collision strength (Ω) for the transition shows extensive resonances with enhanced background resulting in an effective collision strength (Υ) of 2.2 at about 10^4 K that increases to 9.66 around 3×10^5 K. The present results include Ω of all 1431 excitation among the 54 levels and Υ for a limited number of transitions of possible interest. We have found extensive resonances in the low energy region of Ω , convergence of the resonances and of the partial waves with the 54 levels wavefunction. At high energy Ω decreases beyond the resonance region for forbidden transitions, is almost constant or decreases slowly for dipole allowed transitions with low oscillator strengths (f-values), and rises with Bethe-Coulomb behavior of $\ln(E)$ to almost a plateau for transitions with high f-values. The wavefunction of Ca IV was obtained from optimization of 13 configurations $3s^2 3p^5$, $3s 3p^6$, $3s^2 3p^4 3d$, $3s^2 3p^4 4s$, $3s^2 3p^4 4p$, $3s^2 3p^4 4d$, $3s^2 3p^4 4f$, $3s^2 3p^4 5s$, $3s 3p^5 3d$, $3s 3p^5 4s$, $3s 3p^5 4p$, $3p^6 3d$, $3s 3p^4 3d^2$, each with the core configuration of $1s^2 2s^2 2p^6$, using the atomic structure program

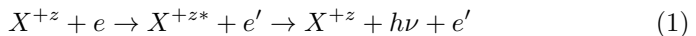
SUPERSTRUCTURE. They produce 387 fine structure levels. We report transition parameters - oscillator strengths, line strength (S) and A -values for a total of 93296 electric dipole (E1), quadrupole (E2), octupole (E3), magnetic dipole (M1) and quadrupole (M2) transitions among these levels. Lifetimes of these levels are also presented.

Keywords: Collisional excitation, Photoexcitation, 3.2 micron line of Ca IV

1 Introduction

Calcium is one of most abundant biogenic elements which is created during supernova (SN) explosions. Lines of Ca I and II are seen in cool stars. The H and K lines and forbidden lines of Ca II are commonly detected in SNe (e.g. [1]). The lines can determine the abundances of the element in the object. Asplund et al [2] obtained Ca abundance in the Sun with respect to hydrogen, in logarithmic abundances, to be $\log[e(\text{Ca})] = 6.34 \pm 0.04$ where $\log[e(\text{Ca})] = 12 + \log[N(\text{Ca})/N(\text{H})]$, H is defined as $\log H = 12.00$, $N(\text{Ca})$ and $N(\text{H})$ are the number densities of elements Ca and H, respectively. Ca-rich supernova, such as, SN 2019ehk in the star forming spiral galaxy Messier 100, about 55 million light years away from the earth, first by Shepherd [3] and analysis by Jacobson-Galan et al [4], brought much attention recently. Jacobson-Galan [4] found that the calcium-rich SN belongs to CaST class. Ca-IV lines in infrared (IR) was observed in NGC 7027 nebula by Feuchtgruber et al. [5]. 3.2 μm line was observed in three Wolf-Rayet stars and was used to determine abundance and wind speed by Ignance et al [6]. Furthermore, emission lines of two calcium ions, Ca-V and Ca-VII, were observed in the NGC 2707 and NGC 6302 nebulae [7], and Ca II lines in the high-temperature environment of white dwarfs [8].

The present work reports study of two atomic processes of Ca IV that produce spectral lines, electron-impact excitation (EIE) and photo-excitation. EIE is one of the most common atomic process in near empty space or in astrophysical plasmas with or without a radiative source. A traveling electron interacts with an ion and transfers part of its energy and promotes the ion to an excited state. It is followed by the target ion de-exciting by emission of a photon, (e.g. [9])



where X^{+z} is the target ion of charge z . The emitted photon can form an observable line depending on the radiative transfer and density of the plasma. The projectile electron can also form a quasi-bound state by exciting the target ion to a higher energy state, E^{**} , while attaching itself to an orbit νl which happens very commonly in nature, matching the energy of a doubly excited

autoionizing Rydberg state

$$E_x \nu l = E^{**}(X^{+z} \nu l) = E_x - z^2 / \nu^2 \quad (2)$$

before going out free. This intermediate state introduces a resonance in the collisional scattering. E_x is the excited energy of the ion, νl are the effective quantum number and angular momentum of the scattered electron. The present study implements close coupling (CC) wavefunction expansion that produces the autoionizing resonances automatically.

The other process, photo-excitation/ de-excitation, forms a line as the ion absorbs or emits a photon

$$X^{+z} + h\nu \leftrightarrow X^{+z*} \quad (3)$$

This process occurs most commonly when there is a radiative source, such as, a star shining the plasma.

Among the low ionization stages of Ca, Ca IV has been the least studied ion. There is no study on electron impact excitation of it found in the literature. EIE of Ca IV is the main focus of the present study.

Among the past studies on energies and transitions, Sugar and Corliss [10] compiled the experimentally measured energy levels of Ca IV which are available at NIST website [11]. The radiative transition rates of Ca IV were reported by Naqvi [12], Varsavsky [13], Fawcett and Gabriel [14], Huang et al [16], Wilson et al. [17], Gabriel et. al [15] who identified several lines generated from observed UV transitions. The probability of detection of Ca IV lines has increased considerably with high resolution observation of James Webb Space Telescope (JWST) in the infra-red region. The present work reports collisional excitation and photo-excitations for many levels of Ca IV which include collision strengths (Ω) and the Maxwellian averaged collision strengths or effective collision strengths (Υ), and parameters f -, S - and A - values for radiative transitions.

2 Theoretical Approximation

We give a brief outline of the theoretical background for electron impact excitation and radiative photo-excitations below as guidance for the readers. More details can be found, e.g. in Pradhan and Nahar [9]. We have treated EIE of Ca IV for collision strengths with relativistic Breit-Pauli R-matrix (BPRM) method, as developed under the Iron Project (IP, [18, 19]). We used a wavefunction expansion in close-coupling (CC) approximation that includes excitation to $n=2,3,4$ levels in the target and obtained collision strengths. We obtained radiative transition parameters for an extensive set of transition using relativistic Breit-Pauli approximation implemented in atomic structure program SUPERSTRUCTURE (SS, [20, 21]).

Although two approaches are used for collision and photo-excitation, the computations are related. BPRM calculations are initiated with the wavefunction expansion of the target ion, e.g. Ca IV, generated by program SUPERSTRUCTURE (SS). We discuss the outlines of collisional excitation first and then photo-excitations or radiative transitions.

2.1 Breit-Pauli R-matrix (BPRM) calculations for EIE

BPRM Hamiltonian as adopted under the Iron Project [18, 19] in atomic Rydberg unit is given by

$$H_{N+1}^{\text{BP}} = \sum_{i=1}^{N+1} \left\{ -\nabla_i^2 - \frac{2Z}{r_i} \right\} + \sum_{j>i}^{N+1} \frac{2}{r_{ij}} + H_{N+1}^{\text{mass}} + H_{N+1}^{\text{Dar}} + H_{N+1}^{\text{so}}. \quad (4)$$

where the first three terms belong to the non-relativistic Hamiltonian and last three terms are the 1-body relativistic corrections which are mass, Darwin, and spin-orbit interaction terms respectively. BPRM codes include all of them and part of the two-body correction terms of the Breit-interaction (e.g. [9]). One Rydberg (Ry) is half of a Hartree giving the factor 2 in the terms.

BPRM calculations start with the target ion wavefunction generated by SS and calculates the wavefunction of the total atomic system of the target ion and the interacting electron in the close coupling (CC) approximation. In CC approximation, the wavefunction of (e+ion) in a state $SL\pi J$, where S is total spin, L is the orbital, and J is the total angular momenta, is expressed as

$$\Psi_E(e + ion) = A \sum_i^n \chi_i(ion)\theta_i + \sum_j c_j \Phi_j(e + ion) \quad (5)$$

In the first term $\chi_i(ion)$ is the wavefunction expansion of the target ion, θ_i is that of the interacting electron, in channel $S_t L_t \pi_t J_t k_i^2 l(SL\pi J)$ where $S_t L_t \pi_t J_t$ is the target ion state interacting with the projectile electron of energy k_i^2 and orbital angular momentum l . The sum represents ground and various excited states of the target ion. A is the anti-symmetrization operator. In the second term, $\Phi_j(e + ion)$ represents the (target+electron) wavefunction, basically part of the first term separated out to show the orthogonality condition of the interacting electron and short range interaction. Close-coupling wave function expansion which includes target ion excitations enables producing the resonances inherently. The interference of the bound states of the target ion and the projectile electron continuum wavefunction in the transition matrix introduces the resonances. Substitution of the CC expansion in the Schrodinger equation with the Breit-Pauli Hamiltonian results in a set of coupled equations. The R-matrix method is used to solve this set of equations for the energy and wavefunctions of the (e+ion) system.

The scattering matrix for transition of the target ion from state i to state k by collision, $\mathbf{S}_{SL\pi J}(S_i L_i J_i l - S_k L_k J_k l')$ where $SL\pi J$ is the (e+ion) state,

l and l' are the incident and scattered partial waves of the free electron, is derived from the reactant matrix of the incident wave (e.g. [9, 23–25]). The collision strength Ω for electron impact excitation (EIE) is given by,

$$\Omega(S_i L_i J_i - S_k L_k J_k) = \frac{1}{2} \sum_{S L \pi J} \sum_{l, l'} (2J + 1) |r \mathbf{S}_{S L \pi J} (S_i L_i J_i l - S_k L_k J_k l')|^2 \quad (6)$$

Ω reveals the detailed features with resonances of the collision. The plasma models use the temperature dependent quantity, the effective collision strengths $\Upsilon(T)$ which is obtained by averaging Ω over Maxwellian distribution function of the electrons at temperature T_e as

$$\Upsilon_{ij}(T_e) = \int_0^\infty \Omega_{ij}(E) \exp(-E/kT_e) d(E/kT_e), \quad (7)$$

where k is the Boltzmann constant and E is the energy of the projectile electron after the excitation, that is, the energy of the scattered electron. The excitation rate coefficient ($q_{ij}(T_e)$) is related to the effective collision strength Υ_{ij} as

$$q_{ij}(T_e) = \frac{8.63 \times 10^{-6}}{g_i T_e^{1/2}} e^{-E_{ij}/kT_e} \Upsilon_{ij}(T_e) \text{ cm}^3/\text{s}, \quad (8)$$

where g_i is the statistical weight of the initial level, T is in K, E_{ij} is the transition energy in Rydberg, and $(1/kT = 157885/T)$.

The high energy background of collision strength shows certain general behaviors depending on the type of excitation. The background of Ω is the smooth curve at the base of resonant features. For forbidden transitions, Ω decreases to almost zero with higher energy. For dipole allowed transitions, using Born approximation with Coulombic wavefunction, Ω shows a high energy limiting behavior and is given by Coulomb-Bethe approximation

$$\Omega_{ij}(E) = \frac{4g_i f_{ij}}{E_{ij}} \ln \frac{E}{E_{ij}}, \quad (9)$$

where f_{ij} is the oscillator strength for a dipole allowed transition, and E is the incident electron energy. In the high energy limit,

$$\Omega_{ij}(E) \sim_{E \rightarrow \infty} d_{ij} \ln(E) \quad (10)$$

where d_{ij} is proportional to the oscillator strength. The logarithmic function will increase with increase in electron energy, but the the rising trend of the function slows down with very high values of the argument. Hence, for a low value of d , Ω is may not change as it is multiplied by a small number. For high value of d , Ω will increase but will lead toward a plateau.

2.2 Atomic structure calculations for radiative transitions

Theoretical details for obtaining radiative transition parameters through atomic structure calculations using program SUPERSTRUCTURE can be found, for example, in [9, 21]. The Hamiltonian includes relativistic mass, Darwin, spin-orbit interaction correction terms, full 2-body Breit interaction and some additional two body terms. The interacting electron and core ion potential, implemented in program SS, is represented by Thomas-Fermi-Amaldi-Dirac potential. The program uses configuration interaction wavefunction expansion, which for a symmetry $J\pi$ can be expressed as

$$\Psi(J\pi) = \sum_{i=1}^N a_i \psi[C_i(J\pi)] \quad (11)$$

where a_i is the amplitude or the mixing coefficient of wavefunction of configuration C_i , $\psi[C_i(J\pi)]$ with symmetry $J\pi$, and the sum is over all N configurations that can produce a level of symmetry $J\pi$. The wavefunction will result in having N number of eigenvalues from the Hamiltonian matrix and each eigenvalue will correspond to energy of one level of the symmetry. Accuracy of the energy of a level may depend on the size of the expansion and identification on the value of the mixing coefficient (e.g. [9].)

The transition matrix element, for example, for electric dipole allowed transition (E1), is given by $\langle \Psi_B || \mathbf{D} || \Psi_{B'} \rangle$ where Ψ_B and $\Psi_{B'}$ are the initial and final state bound wavefunctions, $\mathbf{D} = \sum_i \mathbf{r}_i$ is the dipole operator where the sum is over the number of electrons. The line strength \mathbf{S} is obtained from the mod squared of the transition matrix,

$$\mathbf{S} = \left| \left\langle \Psi_f \left| \sum_{j=1}^{N+1} \mathbf{r}_j \right| \Psi_i \right\rangle \right|^2 \quad (12)$$

where Ψ_i and Ψ_f are the initial and final wavefunctions. The transition parameters, oscillator strength (f_{ij}) and radiative decay rate (A) can be obtained from line strength as

$$f_{ij} = \frac{E_{ji}}{3g_i} \mathbf{S}, \quad A_{ji}(\text{sec}^{-1}) = \left[0.8032 \times 10^{10} \frac{E_{ji}^3}{3g_j} \right] \mathbf{S} \quad (13)$$

Transition probabilities for electric quadrupole (E2), magnetic dipole (M1), electric octupole (E3), magnetic quadrupole (M2) transition parameters can be obtained from their respective line strengths, (e.g. [9, 21]).

Lifetime of an excited level can be obtained from the inverse of the sum of all transition probabilities to lower levels,

$$\tau_i(s) = 1 / \left[\sum_j A_{ji}(s^{-1}) \right] \quad (14)$$

In atomic unit of time $\tau_0 = 2.4191 \times 10^{-17}$ s , the transition probabilities or the radiative decay rate can be expressed as $A_{ji}(s^{-1}) = A_{ji}(a.u.)/\tau_0$.

3 Computation

The R-matrix calculations start with the target wavefunctions as an input. These wavefunctions are obtained from atomic structure calculations, mainly using program SUPERSTRUCTURE (SS) [20, 21]. Ca IV wavefunction, energies and the relevant radiative transition parameters were obtained from an optimized a set of 13 configurations of the ion, $3s^23p^5$, $3s3p^6$, $3s^23p^43d$, $3s^23p^44s$, $3s^23p^44p$, $3s^23p^44d$, $3s^23p^44f$, $3s^23p^45s$, $3s3p^53d$, $3s3p^54s$, $3s3p^54p$, $3p^63d$, $3s3p^43d^2$, with the same core configuration $1s^22s^22p^6$ for each, using SS. The set of optimized Thomas-Fermi orbital scaling parameters are 1.26865(1s), 1.0395(2s), 1.04288(2p), 1.1(3s), 1.1(3p), 1.1(3d), 1.083(4s), 1.079(4p), 1.031(4d), 1.1 (4f), 1.1 (5s) respectively. The configurations set provided 387 fine structure levels, 54 of which were considered for the collisional excitation in the present study and hence used in the wavefunction expansion of Ca IV. Selecting a set of levels of the target or core ion from a large set is the standard for a R-matrix calculation. Computations of collision strengths, which depend on the size of the wavefunction expansion, needed several hundreds of CPU hours on the high performance computers at the Ohio Supercomputer Center.

The purpose of having an optimized set of configurations, which produced a large set of levels, is to ensure contributions from configuration interactions are included in the wavefunctions of levels, and thus can provide a set of levels, starting from the ground level, of higher accuracy for the CC wavefunction expansion. Inclusion of all levels, 387 in the present case, in the calculations will require considerably large computational time, and expected to be computationally prohibitive which is very common, and hence impractical to consider. The set of excited levels considered for a R-matrix calculation is typically based on the expected physics to be revealed, mainly the resonant features. No new physics was expected from levels higher than 54 levels since the resonances would have converged and hence those belonging to higher ones would no longer be strong but have weakened to converge to the background. This was also our finding as demonstrated in the Results section.

Table 1 presents the 54 fine structure levels of Ca IV included in the wavefunction expansion and compares the calculated energies from SS with experimental values tabulated by the National Institute of Standards and Technology (NIST) (www.nist.gov). The comparison shows that the present computed energies are generally within a few percent of the observed values. The accuracy of a level energy depends on the how well the wavefunction expansion is representing the level through interaction of the given set of configurations. For more precise energy positions of the resonances in EIE collision strength, we have replaced the calculated energies with the available observed energies in the BPRM calculations.

Table 1 Comparison of the present calculated energies for the 54 fine structure levels of Ca IV with those (Sugar and Corliss [10]) available in the compilation table of the NIST [11]

K	Configuration	Term	$E_{present}$ (Ry)	E_{NIST} (Ry)	% diff
1	$3s^2 3p^5$	$2P_{3/2}^o$	0	0	0.0
2	$3s^2 3p^5$	$2P_{1/2}^o$	0.0302	0.0284	5.9
3	$3s 3p^6$	$2S_{1/2}$	1.3031	1.3891	6.2
4	$3s^2 3p^4 3d$	$4D_{7/2}$	1.8197	1.8362	0.9
5	$3s^2 3p^4 3d$	$4D_{5/2}$	1.8218	1.8385	0.9
6	$3s^2 3p^4 3d$	$4D_{3/2}$	1.8243	1.8410	0.9
7	$3s^2 3p^4 3d$	$4D_{1/2}$	1.8263	1.8431	0.9
8	$3s^2 3p^4 3d$	$4F_{9/2}$	1.9901	1.9865	0.2
9	$3s^2 3p^4 3d$	$4F_{7/2}$	1.9999	1.9964	0.2
10	$3s^2 3p^4 3d$	$2P_{3/2}$	2.0047	1.9965	0.4
11	$3s^2 3p^4 3d$	$2P_{1/2}$	2.0070	2.0036	0.2
12	$3s^2 3p^4 3d$	$4F_{5/2}$	2.0115	2.0083	0.2
13	$3s^2 3p^4 3d$	$4F_{3/2}$	2.0225	2.0149	0.4
14	$3s^2 3p^4 3d$	$4P_{5/2}$	2.0705	2.0473	0.2
15	$3s^2 3p^4 3d$	$4P_{3/2}$	2.0761	2.0536	1.1
16	$3s^2 3p^4 3d$	$2D_{3/2}$	2.0817	2.0732	0.4
17	$3s^2 3p^4 3d$	$4P_{1/2}$	2.0840	2.0616	1.0
18	$3s^2 3p^4 3d$	$2D_{5/2}$	2.0970	2.0890	0.4
19	$3s^2 3p^4 3d$	$2F_{7/2}$	2.1076	2.1074	0.02
20	$3s^2 3p^4 3d$	$2F_{5/2}$	2.1310	2.1297	0.06
21	$3s^2 3p^4 3d$	$2G_{7/2}$	2.1369	2.1573	0.95
22	$3s^2 3p^4 3d$	$2G_{9/2}$	2.1382	2.1571	0.88
23	$3s^2 3p^4 3d$	$2F_{7/2}$	2.2990	2.3051	0.26
24	$3s^2 3p^4 3d$	$2F_{5/2}$	2.3046	2.3109	0.27
25	$3s^2 3p^4 3d$	$2D_{5/2}$	2.4602	2.4937	1.36
26	$3s^2 3p^4 3d$	$2D_{3/2}$	2.4653	2.4993	1.34
27	$3s^2 3p^4 3d$	$2S_{1/2}$	2.6559	2.6979	1.8
28	$3s^2 3p^4 4s$	$4P_{5/2}$	2.6688	2.7714	3.7
29	$3s^2 3p^4 4s$	$4P_{1/2}$	2.6701	2.7972	4.5
30	$3s^2 3p^4 4s$	$2P_{3/2}$	2.6780	2.7974	4.24
31	$3s^2 3p^4 4s$	$4P_{3/2}$	2.6818	2.7857	3.6
32	$3s^2 3p^4 4s$	$2P_{1/2}$	2.6895	2.8098	4.3
33	$3s^2 3p^4 3d$	$2D_{5/2}$	2.7449	2.8566	4.2
34	$3s^2 3p^4 3d$	$2P_{3/2}$	2.7495	2.8976	5.2
35	$3s^2 3p^4 3d$	$2P_{1/2}$	2.7666	2.9135	4.9
36	$3s^2 3p^4 4s$	$2D_{3/2}$	2.7689	2.8794	3.8
37	$3s^2 3p^4 4s$	$2D_{5/2}$	2.8479	2.9941	4.7
38	$3s^2 3p^4 3d$	$2D_{3/2}$	2.8491	2.9961	4.7
39	$3s^2 3p^4 4p$	$4P_{5/2}^o$	3.0145	3.1268	3.8
40	$3s^2 3p^4 4p$	$4P_{3/2}^o$	3.0179	3.1318	3.5
41	$3s^2 3p^4 4p$	$4P_{1/2}^o$	3.0251	3.1386	3.5
42	$3s^2 3p^4 4p$	$4D_{7/2}^o$	3.0539	3.1829	4.1
43	$3s^2 3p^4 4p$	$4D_{5/2}^o$	3.0610	3.1913	4.0
44	$3s^2 3p^4 4p$	$4D_{3/2}^o$	3.0706	3.1996	4.0
45	$3s^2 3p^4 4p$	$2P_{1/2}^o$	3.0729	3.2128	4.3
46	$3s^2 3p^4 4p$	$4D_{1/2}^o$	3.0751	3.2039	4.0
47	$3s^2 3p^4 4p$	$2D_{5/2}^o$	3.0824	3.2185	4.0
48	$3s^2 3p^4 4s$	$2S_{1/2}$	3.0828	3.2573	5.4
49	$3s^2 3p^4 4p$	$2D_{3/2}^o$	3.0888	3.2376	4.0
50	$3s^2 3p^4 4p$	$2P_{3/2}^o$	3.1017	3.2209	3.7
51	$3s^2 3p^4 4p$	$4S_{3/2}^o$	3.1217	3.2577	4.0
52	$3s^2 3p^4 4p$	$2S_{1/2}^o$	3.1249	3.2598	4.0
53	$3s^2 3p^4 4p$	$2F_{7/2}^o$	3.2091	3.3629	4.5
54	$3s^2 3p^4 4p$	$2F_{5/2}^o$	3.2133	3.3591	4.5

It is important to ensure convergence in contributions by the number of partial waves and (e+ion) symmetries to the collision strengths Ω . We computed Ω several times by varying different sets of partial waves l going up to 22 and (e-ion) symmetries J going up to ≤ 22 of even and odd parities. We found that i) Ω background is converged with the highest values of $l = 20$ and $J\pi = 11$, ii) larger number of l and $J\pi$ than these introduced computational instability which gives NaN (Not a Number) for the collision strengths at various electron energies.

Getting "NaN" for Ω values is a known problem for a R-matrix calculation. They are introduced when the computation goes through very small numbers. Usually the NaN points are deleted from the sets of Ω values. However, we made attempts to get approximate values Ω at energies of NaN values obtained with large l and J values by extrapolating or interpolating the neighboring Ω points. Smooth background can be extrapolated but resonances are not reproduced in Ω as can be seen in the blue (with extrapolation) and red curves (no extrapolation) in Figure 1 representing the same excitation of the ion. The resonant peaks of the blue curve, which has many NaN points and interpolation was carried out to replace the NaNs with real numbers, are lower than the red curves.

Figure 1 also demonstrates the test of convergence of Ω for a few sets of highest values of l and J for the excitations of a) ${}^2P_{3/2}^o - {}^2P_{1/2}^o$ and b) ${}^2P_{1/2}^o - {}^2S_{1/2}$ computed at a coarse energy mesh. The red curves correspond to use of $l = 0 - 20$ and $J\pi = 0 - 11$, the blue ones to $l = 0 - 22$ and $J\pi = 0 - 21$ and the magenta ones to $l = 0 - 11$ and $J\pi = 0 - 10$. Ω in magenta ($l = 0 - 11$ and $J\pi = 0 - 10$) are considerably lower than the other curves indicating that convergence of contributions from 12 partial waves has not been reached. The blue and the red curves have about the same background indicating convergence in contributions of partial waves has reached. Hence specifications for the red curve, $l = 0 - 20$ and $J\pi = 0 - 11$, have been used for the computation of Ω . Final Ω values were obtained at fine energy meshes. We used a very fine energy mesh of $\Delta E < 10^{-6}$ Rydberg to resolve the near-threshold resonances.

The above discussion concerns impact of partial waves that are noticeable. Beyond it, top-up which gives some additional contributions is added. As top-up contributions, we included contributions of higher multipole potentials to Ω using the option `ipert=1` in STGF of the R-matrix codes. The other top-up contribution can come from higher partial waves, beyond the specified ones, using the option chosen as `ipert=2`, in STGF. The approximation incorporated in the R-matrix code STGF is most probably based on the treatment of Burgess and Tully [22] of higher partial waves. However, computation of contributions of the higher partial waves, not only takes much longer time, it is not done for most cases as it stops due to numerical issues except for a few excitations and at some energies. We computed contributions of higher partial waves when it is possible to test them and found negligible contributions in increasing the Ω values to affect the average collision strengths Υ . The problem is compensated,

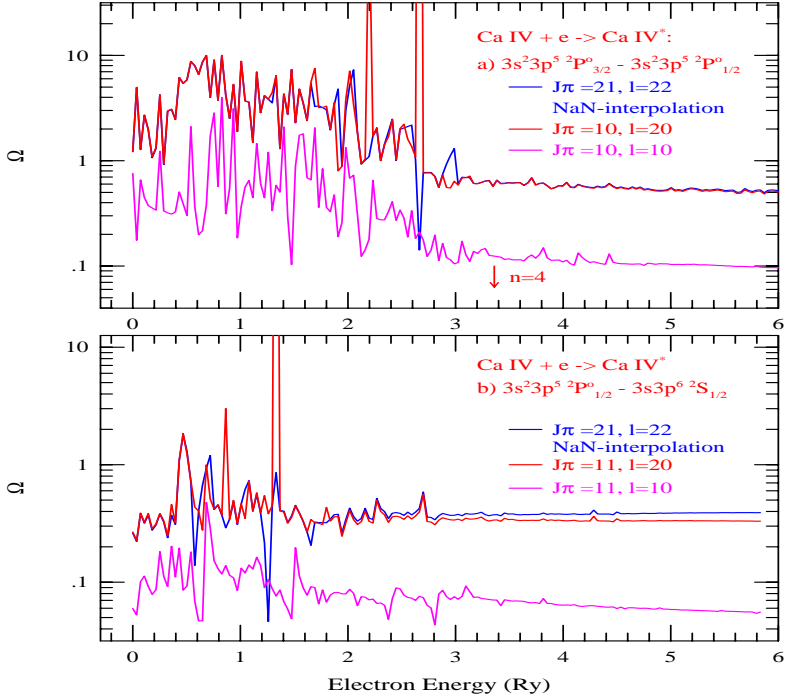


Fig. 1 Demonstration of convergence of contributions of partial waves with various l and J values to Ω . The x-axis corresponds to the energy of the scattered electron after the excitation which starts with zero energy. Red curves indicate the best convergent condition.

as done in the present case, by including larger number of partial waves without the approximation.

Program "ecs-omg.f" [26] was used to calculate the effective collision strengths Υ , Eq.(7), at various temperatures where Ω is integrated over the energy of the scattered electron from zero to a high value. The high energy limit is chosen to a value at which Ω has diminished to a near zero value or has reached a plateau and the exponential factor of Υ has approached a near zero value. Ω points between the highest electron energy computed by the BPRM codes to the highest energy limit of the Υ integral are obtained using the logarithmic behavior of Coulomb-Bethe approximation of Eq.(10).

The radiative data of f - and A -values for dipole allowed photo-excitations (E1) have been reprocessed with experimental energies using code PRCS (e.g. [?]). This allows to obtain the transition parameters at observed wavelengths. For the reprocessing, the transition energies were obtained from the experimental level energies and then multiplied, following Eq. 13. to the calculated line strengths from code SUPERSTRUCTURE. For the levels for which no observed or measured values are available, calculated energies were used.

4 Results and Discussions

We present atomic parameters for electron impact excitation of ($e + \text{Ca IV} \rightarrow \text{Ca IV}^* + e' \rightarrow \text{Ca IV} + h\nu + e'$) and photo-excitation of ($\text{Ca IV} + h\nu \leftrightarrow \text{Ca IV}^*$). The results for the collisional excitation are reported for the first time, as indicated by literature search. They are described below first followed by those for photoexcitation.

4.1 Collisional excitation of Ca IV

We discuss the characteristic features of collisional excitation with illustrative examples. The first excitation of the target is usually of particular interest because of its high probability through EIE and the emitted photon, typically of low energy, can travel for a long time without being absorbed. If the corresponding emission line is strong, it can be detected easily in low density plasmas and be used for identification of the ion and environmental diagnostics. The first excitation in Ca IV, $3p^5 \ ^2P_{3/2}^o - 3p^5 \ ^2P_{1/2}^o$, within the ground configuration is of particular importance since the wavelength of the emission line, $3.207 \ \mu\text{m}$, is well within the high resolution IR wavelength detection range, $0.6 - 28.3 \ \mu\text{m}$, of JWST, and could be used for diagnostics, abundances (e.g. [6]).

Figure 2 upper panel presents collision strength for the first excitation $\Omega(^2P_{3/2}^o - ^2P_{1/2}^o)$ of the target ion Ca IV with respect to scattered electron energy after the excitation. The electron energy is relative to the excitation threshold and hence starts at zero. We note that the Ω for the collisional excitation is quite strong as it shows extensive resonances with enhanced background in the energy region between the first excited level $^2P_{1/2}^o$ and the next one $^2S_{1/2}$ (pointed by arrows), and continues to be strong beyond it up to $^2D_{3/2}$ level, the one before the last dipole allowed transition in the 54 level wavefunction expansion. Beyond, $^2D_{3/2}$ the transitions are forbidden except one and the resonances become weaker. There are 29 dipole allowed levels in total that exist in this energy range. Each excitation of the target ion corresponds to a Rydberg series of resonances. Typically, the resonances corresponding to a dipole allowed excitation are visible while others are suppressed. The resonances belonging to very high energy levels are found to become weaker. Such weakening trend indicates convergence of resonant contributions to the collisional parameters.

Figure 2 lower panel presents effective collision strength (Υ) for $\Omega[(^2P_{3/2}^o - ^2P_{1/2}^o)]$. Starting low at lower energy, Υ forms a shoulder bump at 10^4 K. Then it rises relatively quickly reaching to the high peak value 9.66 at about 3×10^5 K. The peak indicates existence of a strong line of the transition in Ca IV which can be detected. The intensity of the line will depend on the plasma environment.

We present illustrative examples of forbidden transitions in Ca IV. Figure 3 presents collision strengths for two forbidden excitations in Ca IV, a)

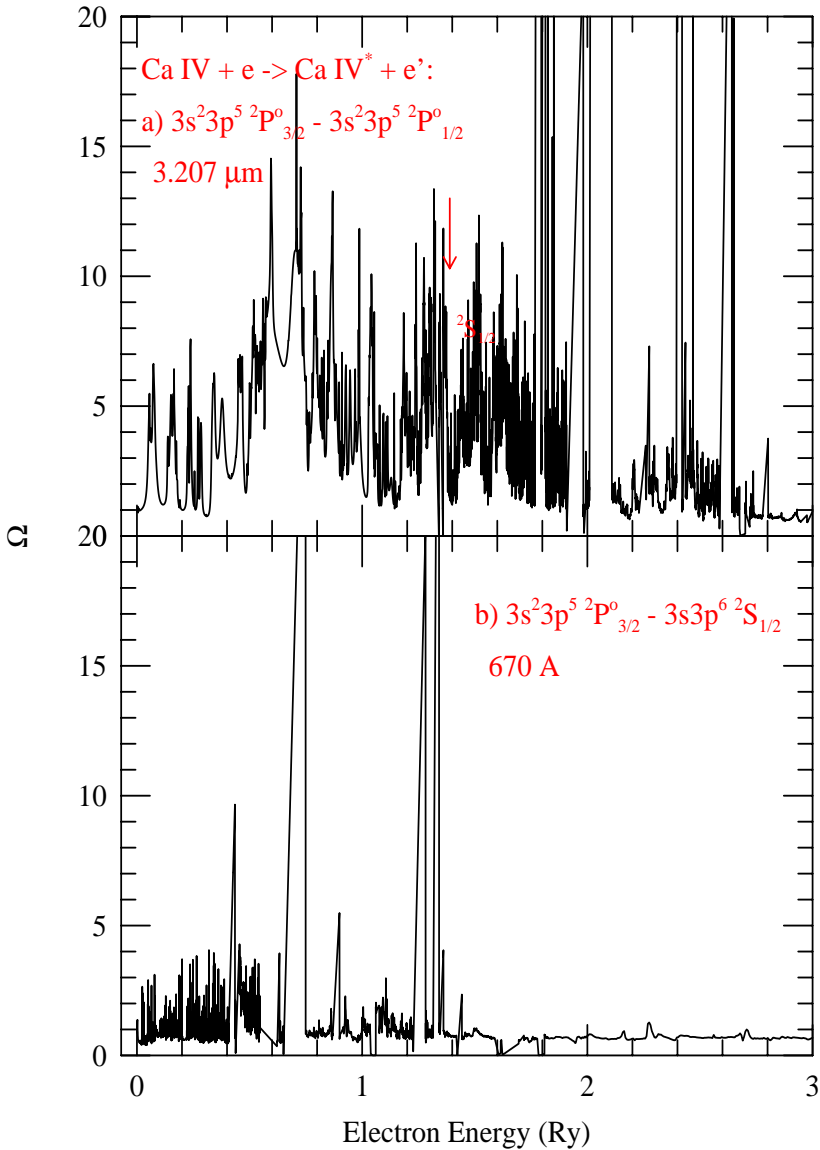


Fig. 2 Upper panel: EIE collision strength (Ω) of Ca IV for the first excitation $3s^2 3p^5 \ ^2P_{3/2}^o - 3s^2 3p^5 \ ^2P_{1/2}^o$ of the ground level with respect to scattered electron energy in Ry unit. Extensive resonances with enhanced background can be noted within the energy region of dipole allowed transitions from the ground level $3s^2 3p^5 \ ^2P_{3/2}^o$ up to $^2D_{1/2}^o$. Lower panel: Effective collision strength for $3s^2 3p^5 \ ^2P_{3/2}^o - 3s^2 3p^5 \ ^2P_{1/2}^o$ excitation in Ca IV showing a high peak value at about 3×10^5 K indicating high probability of detection of the line by JWST.

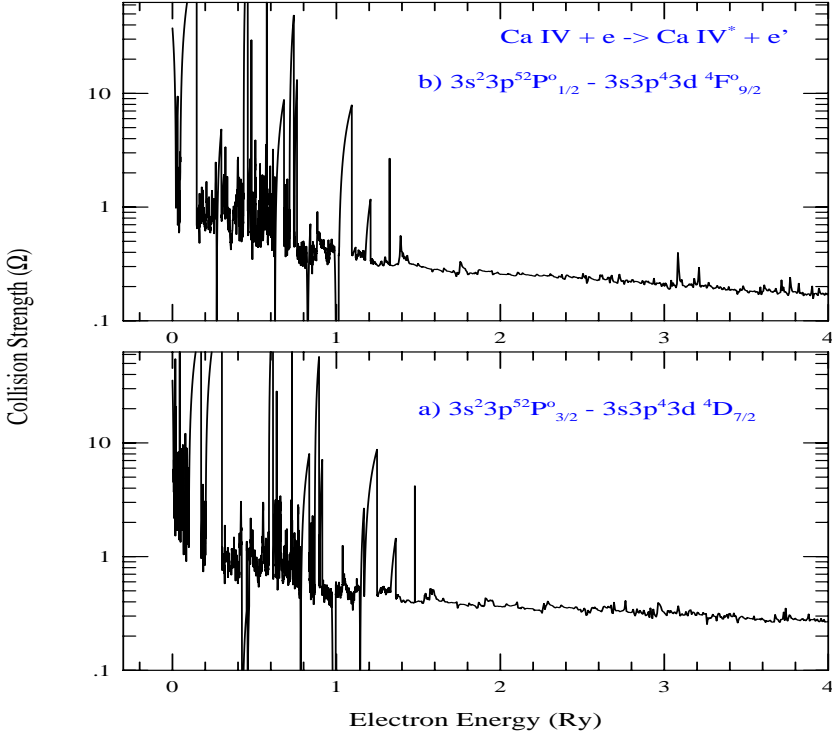


Fig. 3 Collision strength for forbidden excitation a) $\Omega(3s^23p^5\ ^2P_{3/2}^o - 3s^23p^44s\ ^4D_{7/2})$ and b) $\Omega(3s^23p^5\ ^2P_{3/2}^o - 3s^23p^44s\ ^4F_{9/2})$ in extreme ultraviolet, 496 Å and 458 Å respectively, illustrating resonant features in the low energy region and decreasing background in the high energy region.

$\Omega(3s^23p^5\ ^2P_{3/2}^o - 3s^23p^44s^4D_{7/2})$ and b) $\Omega(3s^23p^5\ ^2P_{3/2}^o - 3s^23p^44s^4F_{9/2})$. Both transitions show presence of strong resonances in the lower energy region. The resonances become weaker in higher energy region indicating contribution of resonances is converging. This is the typical trend of Ω for forbidden transitions. Both of these transitions lie in the extreme ultraviolet region with wavelengths of 496 and 458 Å respectively.

Collision strengths for dipole allowed transitions may show a different trend in the high energy background from those of forbidden transitions. The dipole in the target can affect the partial waves of the incident electron and contribute to the collision strength. The contribution depends on the oscillator strength for the dipole transition. For stronger transitions, inclusion of larger number of partial waves is important for converged contributions.

Figure 4 presents features of Ω (EIE) for two dipole allowed transitions to low lying excited levels, a) $3s^23p^5\ ^2P_{1/2}^o - 3s3p^6\ ^2S_{1/2}$ (levels 2-3) at 670

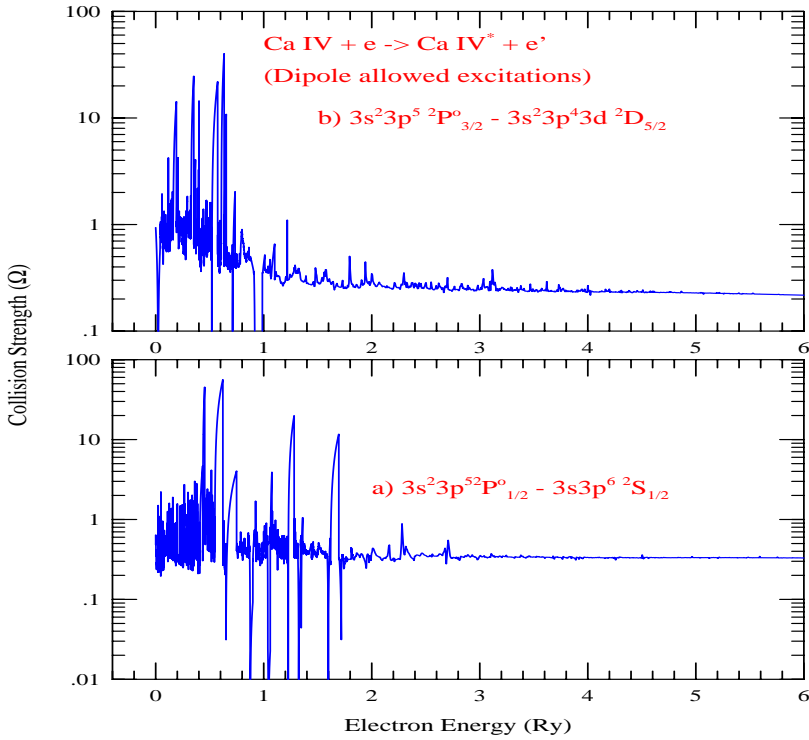


Fig. 4 Features of $\Omega(EIE)$ for two weaker dipole allowed transitions (oscillator strengths are given in Table 2): a) $3s^23p^5\ ^2P_{1/2}^o - 3s3p^6\ ^2S_{1/2}$ (levels 2-3) and b) relatively higher transition $3s^23p^5\ ^2P_{3/2}^o - 3s^23p^43d^2D_{5/2}$ (levels 1-18). Resonances have converged to a smooth background at high energy where the background remains almost constant or decreases slowly with increase of energy, typical for weak transitions.

\AA and b) $3s^23p^5\ ^2P_{3/2}^o - 3p^43d\ ^2D_{5/2}$ (levels 1-18) at $435\ \text{\AA}$. Ω for these transitions show presence of prominent resonances in the lower energy regions which become weaker converging to smooth background at higher energy. It can be noted that the high energy background is decreasing very slowly or remaining almost constant. These transitions are much weaker compared to others as indicated by their smaller values for the oscillator strengths and A -values presented in Table 2.

Figure 5 presents Ω for dipole allowed excitation of a) $3s^23p^5\ ^2P_{3/2}^o - (3s^23p^43d)^2D_{5/2}$ at $340\ \text{\AA}$ and b) $3s^23p^5\ ^2P_{3/2}^o - (3s^23p^44s)^2P_{3/2}$ at $332\ \text{\AA}$ in Ca IV. The high peak resonances are converging near 1 Ry. Although there are much more core ion excitations included in the wavefunction expansion, the Rydberg series of resonances belonging to them have become weak with almost no contributions to Ω . This indicates convergence in the wavefunction

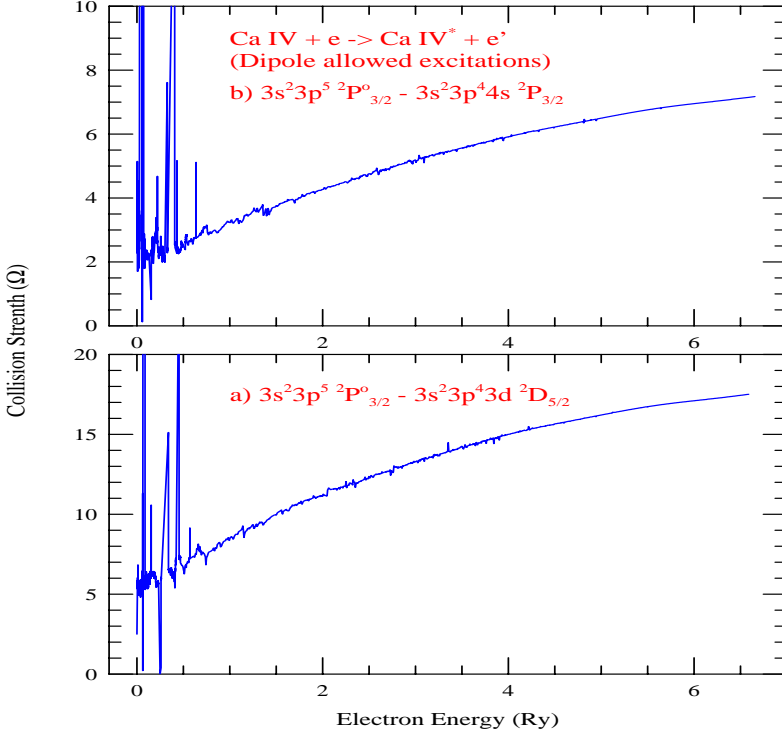


Fig. 5 Features of Ω for excitation to high lying dipole allowed levels, a) $3s^23p^5\ ^2P_{3/2}^o - (3s^23p^43d)^2D_{5/2}$ and b) $3s^23p^5\ ^2P_{3/2}^o - (3s^23p^44s)^2P_{3/2}$ with stronger or larger values for oscillator strengths illustrating (a) convergence of resonances and (b) rising Coulomb-Bethe $\ln(E)$ behavior of Ω at higher energy. The background of Ω rises toward forming a plateau.

expansion for generating resonant features. However, the background of Ω is rising with energy toward forming a plateau. This trend is in agreement with the expected Coulomb-Bethe behavior of $\Omega_{if}(E) \sim_{E \rightarrow \infty} d \ln(E)$ (Eq.10) at high energy for transitions with stronger or larger values for oscillator strength or A -values. The f - and A -values for for the two transitions are given in Table 2. As discussed above, for these transitions, larger number of partial waves needs to be considered in calculating Ω . The rising trend toward a plateau may not result in with inadequate number of partial waves. In such case, Ω is often extrapolated with Coulomb-Bethe form.

Astrophysical models require temperature dependent effective collision strength (Υ). Table 3 presents Υ for some excitations to levels that could be of importance for astrophysical applications. Υ for any other excitation of the 1431 transitions can be computed by averaging Ω over Maxwellian distribution

Table 2 Dipole allowed transitions between levels i and j , their f and A-values, and transition wavelength λ_{ij} in Angstrom unit for the illustrated examples of Ω of Ca IV in Figures 4 and 5. The level indices i and j correspond to those in Table 1.

Figure	i - j	$SL\pi J$		λ_{ij} (Å)	f_{ij}	$A_{ji}(\text{s}^{-1})$
		i	j			
4a	2 - 3	$2P_{1/2}^o$	$2S_{1/2}$	670	1.55E-02	2.01E+08
4b	1 -18	$2P_{3/2}^o$	$2D_{5/2}$	435	8.14E-03	1.98E+08
5a	1 -33	$2P_{3/2}^o$	$2D_{5/2}$	319	2.60E+00	1.14E+11
5b	1 -30	$2P_{3/2}^o$	$2P_{3/2}$	332	1.09E+00	7.10E+10

function at any temperature. The Ω values, and Υ for a number of excitations, in addition to the ones presented here, are available electronically at NORAD-Atomic-Data [27].

4.2 Energy levels and radiative transition parameters of Ca IV

We present about 93000 radiative transition rates for Ca IV obtained from atomic structure calculations in Breit-Pauli approximation implemented in code SUPERSTRUCTURE. The 13 configurations of Ca IV, listed in Computation section, resulted in 387 fine structure energy levels, and 93,296 radiative transitions of types allowed (E1) and forbidden (E2, E3, M1, M2).

Our calculated energies for Ca IV have been compared with the measured values in Table 1 in the Computation section. They are in good agreement with the observed energies available at NIST table. As seen in Table 1, the differences between calculated and measured energies are within 5% for most of the levels except for the highest lying $4D^o$ and $4F^o$ states where the differences are about 8%.

The A-values have been benchmark with limited number of available data. The present transition probabilities are compared, in Table 4, with the only 3 available A-values in the NIST compilation, and with those available from other sources. Transition $3s^23p^5(2P_{3/2}^o) \rightarrow 3s^23p^5(2P_{1/2}^o)$ can be both M1 and E2 types. The present A-value for the M1 transition, 0.545, is in excellent agreement with 0.543 of Naqvi [12]. The present value is also in good agreement with, 0.379 by Huang et al [16] given the typical magnitude of A-values of the order of 10^8 s^{-1} or higher for E1 transitions. Similarly for the very weak E2 transition, the present A-value, $3.82\text{e-}05 \text{ sec}^{-1}$ is also in very good agreement with, $1.906\text{E-}05 \text{ sec}^{-1}$, of Huang et al [16]. For the first dipole allowed transitions $3s^23p^5(2P_{3/2,1/2}^o) \rightarrow 3s3p^6(2S_{1/2})$ present A-values agree very well with those of Wilson et al [17], but differ from Huang et al and Varsavsky [13] who also differ from each other and from Wilson et al. As Table 4 shows, the present results are in agreement with those of Wilson et al for other transitions.

We are providing two calculated A-values for the dipole allowed transitions in order to compare the accuracy, the first A-value has been obtained using

Table 3 Υ at various temperatures for different excitations of levels 1-2 to 1-18 in Ca IV.

logT	T (K)	Υ : 1- 2	1- 3	2- 3	1- 4	1- 5
2.00	1.000E+02	9.312E-01	1.038E+00	5.709E-01	3.274E+01	2.158E-01
2.10	1.265E+02	9.339E-01	1.061E+00	5.674E-01	3.199E+01	2.395E-01
2.20	1.600E+02	9.382E-01	1.075E+00	5.587E-01	3.104E+01	2.827E-01
2.31	2.024E+02	9.439E-01	1.077E+00	5.447E-01	2.986E+01	3.545E-01
2.41	2.560E+02	9.507E-01	1.065E+00	5.261E-01	2.841E+01	4.608E-01
2.51	3.237E+02	9.581E-01	1.040E+00	5.037E-01	2.669E+01	6.014E-01
2.61	4.095E+02	9.654E-01	1.002E+00	4.791E-01	2.474E+01	7.688E-01
2.71	5.179E+02	9.722E-01	9.568E-01	4.537E-01	2.261E+01	9.507E-01
2.82	6.551E+02	9.785E-01	9.081E-01	4.294E-01	2.042E+01	1.134E+00
2.92	8.286E+02	9.851E-01	8.608E-01	4.081E-01	1.826E+01	1.315E+00
3.02	1.048E+03	9.948E-01	8.192E-01	3.909E-01	1.623E+01	1.503E+00
3.12	1.326E+03	1.014E+00	7.854E-01	3.784E-01	1.440E+01	1.724E+00
3.22	1.677E+03	1.054E+00	7.604E-01	3.702E-01	1.284E+01	2.002E+00
3.33	2.121E+03	1.127E+00	7.436E-01	3.654E-01	1.156E+01	2.335E+00
3.43	2.683E+03	1.242E+00	7.345E-01	3.634E-01	1.055E+01	2.690E+00
3.53	3.393E+03	1.395E+00	7.321E-01	3.635E-01	9.865E+00	3.018E+00
3.63	4.292E+03	1.572E+00	7.354E-01	3.655E-01	9.610E+00	3.292E+00
3.73	5.429E+03	1.752E+00	7.433E-01	3.694E-01	9.976E+00	3.553E+00
3.84	6.866E+03	1.920E+00	7.551E-01	3.750E-01	1.113E+01	3.947E+00
3.94	8.685E+03	2.064E+00	7.705E-01	3.844E-01	1.312E+01	4.689E+00
4.04	1.099E+04	2.185E+00	7.909E-01	4.056E-01	1.577E+01	5.927E+00
4.14	1.389E+04	2.294E+00	8.220E-01	4.587E-01	1.869E+01	7.609E+00
4.24	1.758E+04	2.411E+00	8.747E-01	5.748E-01	2.139E+01	9.464E+00
4.35	2.223E+04	2.560E+00	9.640E-01	7.800E-01	2.341E+01	1.113E+01
4.45	2.812E+04	2.759E+00	1.101E+00	1.073E+00	2.448E+01	1.232E+01
4.55	3.556E+04	3.016E+00	1.285E+00	1.419E+00	2.455E+01	1.288E+01
4.65	4.498E+04	3.353E+00	1.497E+00	1.762E+00	2.373E+01	1.282E+01
4.76	5.690E+04	3.841E+00	1.708E+00	2.047E+00	2.222E+01	1.224E+01
4.86	7.197E+04	4.576E+00	1.886E+00	2.241E+00	2.024E+01	1.130E+01
4.96	9.103E+04	5.599E+00	2.007E+00	2.331E+00	1.803E+01	1.015E+01
5.06	1.151E+05	6.818E+00	2.060E+00	2.323E+00	1.574E+01	8.907E+00
5.16	1.456E+05	8.028E+00	2.045E+00	2.234E+00	1.353E+01	7.674E+00
5.27	1.842E+05	8.996E+00	1.975E+00	2.088E+00	1.147E+01	6.514E+00
5.37	2.330E+05	9.559E+00	1.865E+00	1.907E+00	9.610E+00	5.464E+00
5.47	2.947E+05	9.661E+00	1.733E+00	1.711E+00	7.982E+00	4.541E+00
5.57	3.728E+05	9.347E+00	1.592E+00	1.516E+00	6.583E+00	3.745E+00
5.67	4.715E+05	8.718E+00	1.453E+00	1.332E+00	5.398E+00	3.072E+00
5.78	5.964E+05	7.893E+00	1.324E+00	1.165E+00	4.408E+00	2.509E+00
5.88	7.543E+05	6.978E+00	1.207E+00	1.018E+00	3.589E+00	2.044E+00
5.98	9.541E+05	6.058E+00	1.105E+00	8.908E-01	2.917E+00	1.663E+00
6.08	1.207E+06	5.187E+00	1.017E+00	7.837E-01	2.370E+00	1.352E+00
6.18	1.526E+06	4.398E+00	9.435E-01	6.943E-01	1.927E+00	1.101E+00
6.29	1.931E+06	3.705E+00	8.822E-01	6.205E-01	1.570E+00	8.981E-01
6.39	2.442E+06	3.112E+00	8.317E-01	5.602E-01	1.283E+00	7.353E-01
6.49	3.089E+06	2.612E+00	7.906E-01	5.113E-01	1.053E+00	6.050E-01
6.59	3.907E+06	2.198E+00	7.572E-01	4.718E-01	8.700E-01	5.010E-01
6.69	4.942E+06	1.857E+00	7.303E-01	4.400E-01	7.238E-01	4.181E-01
6.80	6.251E+06	1.579E+00	7.087E-01	4.146E-01	6.075E-01	3.521E-01
6.90	7.906E+06	1.354E+00	6.914E-01	3.942E-01	5.151E-01	2.997E-01
7.00	1.000E+07	1.173E+00	6.776E-01	3.780E-01	4.417E-01	2.580E-01
logT	T (K)	Υ : 1- 6	1- 7	1-12	1-13	1-18
2.00	1.000E+02	1.307E+00	4.810E-01	4.444E-01	8.154E-01	9.113E-01
2.10	1.265E+02	1.221E+00	4.936E-01	4.540E-01	8.560E-01	9.043E-01
2.20	1.600E+02	1.164E+00	5.075E-01	4.647E-01	9.006E-01	8.956E-01
2.31	2.024E+02	1.136E+00	5.222E-01	4.758E-01	9.425E-01	8.845E-01
2.41	2.560E+02	1.131E+00	5.374E-01	4.866E-01	9.756E-01	8.705E-01
2.51	3.237E+02	1.147E+00	5.526E-01	4.963E-01	9.969E-01	8.528E-01
2.61	4.095E+02	1.175E+00	5.670E-01	5.042E-01	1.008E+00	8.304E-01
2.71	5.179E+02	1.210E+00	5.797E-01	5.102E-01	1.014E+00	8.023E-01
2.82	6.551E+02	1.246E+00	5.902E-01	5.195E-01	1.028E+00	7.675E-01
2.92	8.286E+02	1.285E+00	5.983E-01	5.546E-01	1.077E+00	7.260E-01

Table 3 continues

logT	T (K)	T: 1- 6	1- 7	1-12	1-13	1-18
3.02	1.048E+03	1.335E+00	6.038E-01	6.781E-01	1.206E+00	6.795E-01
3.12	1.326E+03	1.414E+00	6.065E-01	1.021E+00	1.485E+00	6.321E-01
3.22	1.677E+03	1.533E+00	6.080E-01	1.804E+00	2.005E+00	5.891E-01
3.33	2.121E+03	1.690E+00	6.163E-01	3.326E+00	2.872E+00	5.558E-01
3.43	2.683E+03	1.873E+00	6.615E-01	5.914E+00	4.173E+00	5.359E-01
3.53	3.393E+03	2.079E+00	8.171E-01	9.770E+00	5.920E+00	5.317E-01
3.63	4.292E+03	2.336E+00	1.199E+00	1.478E+01	7.988E+00	5.465E-01
3.73	5.429E+03	2.688E+00	1.911E+00	2.039E+01	1.011E+01	5.866E-01
3.84	6.866E+03	3.169E+00	2.955E+00	2.576E+01	1.198E+01	6.590E-01
3.94	8.685E+03	3.769E+00	4.202E+00	3.003E+01	1.332E+01	7.674E-01
4.04	1.099E+04	4.427E+00	5.432E+00	3.264E+01	1.402E+01	9.097E-01
4.14	1.389E+04	5.047E+00	6.429E+00	3.343E+01	1.406E+01	1.080E+00
4.24	1.758E+04	5.531E+00	7.061E+00	3.259E+01	1.357E+01	1.273E+00
4.35	2.223E+04	5.813E+00	7.294E+00	3.053E+01	1.268E+01	1.480E+00
4.45	2.812E+04	5.870E+00	7.175E+00	2.768E+01	1.154E+01	1.685E+00
4.55	3.556E+04	5.718E+00	6.789E+00	2.446E+01	1.029E+01	1.865E+00
4.65	4.498E+04	5.401E+00	6.230E+00	2.117E+01	9.026E+00	1.993E+00
4.76	5.690E+04	4.969E+00	5.576E+00	1.802E+01	7.809E+00	2.053E+00
4.86	7.197E+04	4.469E+00	4.890E+00	1.514E+01	6.679E+00	2.038E+00
4.96	9.103E+04	3.942E+00	4.216E+00	1.258E+01	5.656E+00	1.956E+00
5.06	1.151E+05	3.420E+00	3.583E+00	1.036E+01	4.749E+00	1.825E+00
5.16	1.456E+05	2.926E+00	3.009E+00	8.470E+00	3.957E+00	1.663E+00
5.27	1.842E+05	2.474E+00	2.502E+00	6.885E+00	3.277E+00	1.487E+00
5.37	2.330E+05	2.072E+00	2.064E+00	5.571E+00	2.700E+00	1.312E+00
5.47	2.947E+05	1.722E+00	1.691E+00	4.490E+00	2.215E+00	1.145E+00
5.57	3.728E+05	1.423E+00	1.378E+00	3.608E+00	1.812E+00	9.941E-01
5.67	4.715E+05	1.170E+00	1.118E+00	2.892E+00	1.479E+00	8.604E-01
5.78	5.964E+05	9.593E-01	9.047E-01	2.314E+00	1.207E+00	7.448E-01
5.88	7.543E+05	7.849E-01	7.303E-01	1.849E+00	9.842E-01	6.467E-01
5.98	9.541E+05	6.418E-01	5.888E-01	1.477E+00	8.038E-01	5.646E-01
6.08	1.207E+06	5.252E-01	4.744E-01	1.179E+00	6.582E-01	4.965E-01
6.18	1.526E+06	4.307E-01	3.824E-01	9.408E-01	5.410E-01	4.407E-01
6.29	1.931E+06	3.544E-01	3.087E-01	7.513E-01	4.471E-01	3.953E-01
6.39	2.442E+06	2.931E-01	2.497E-01	6.007E-01	3.719E-01	3.585E-01
6.49	3.089E+06	2.440E-01	2.027E-01	4.809E-01	3.119E-01	3.288E-01
6.59	3.907E+06	2.047E-01	1.652E-01	3.859E-01	2.641E-01	3.050E-01
6.69	4.942E+06	1.734E-01	1.354E-01	3.106E-01	2.261E-01	2.859E-01
6.80	6.251E+06	1.485E-01	1.117E-01	2.508E-01	1.959E-01	2.707E-01
6.90	7.906E+06	1.287E-01	9.292E-02	2.035E-01	1.719E-01	2.586E-01
7.00	1.000E+07	1.129E-01	7.802E-02	1.661E-01	1.529E-01	2.490E-01

the experimental transition energy and the second one, below it, using the calculated energy. We can see that they themselves do not differ significantly from each other. Some differences among the results are expected due to use of different optimization of the configurations included in each calculations and the accuracy in the methods considered for calculations of the transition parameters.

The present work provides lifetimes of all 386 excited levels in a file that is available electronically at NORAD-Atomic-Data [27]. Lifetime of an excited level can be calculated if the A-values or the radiative decay rates of the level to the lower levels are known. Lifetimes are measurable at experimental set-ups. Table 5 presents lifetimes of a few levels to illustrate their values. For each excited level in the table, the level number, configuration number, spectroscopic notation and energy are given. This line is followed by the A-values of the level decaying to lower levels. The A-values are added and the sum is inverted to obtain the lifetime. Levels decaying through the forbidden

Table 4 Comparison of present A-values for Ca-IV with those available in literature. For the E1 transitions, the first A-value from the present work represents use of experimental transition energy while the second one (below it) of calculated energy. K, KP are the initial and final transitional energy level indices (as given in Table 1), λ is the transition wavelength in Å unit. The references are given in superscripts.

K	KP	λ (Å)	Transition	A(Present) (sec ⁻¹)	A(Others) (sec ⁻¹)
1	2		$3s^23p^5(^2P_{3/2}^o) \rightarrow 3s^23p^5(^2P_{1/2}^o)$	M1:0.545	M1:0.541 ^[12] ,0.3786 ^[16]
1	2		$3s^23p^5(^2P_{3/2}^o) \rightarrow 3s^23p^5(^2P_{1/2}^o)$	E2:3.82e-5	E2:1.906E-5 ^[16]
1	3	656	$3s^23p^5(^2P_{3/2}^o) \rightarrow 3s3p^6(^2S_{1/2})$	5.11E+8 4.22E+8	7.425E+8 ^[17] ,1.20E+10 ^[13] , 1.09e+10 ^[16]
2	3	669.7	$3s^23p^5(^2P_{1/2}^o) \rightarrow 3s3p^6(^2S_{1/2})$	2.466E+8 2.01E+8	3.529E+8 ^[17] , 5.4E+9 ^[13]
1	10	454.6	$3s^23p^5(^2P_{3/2}^o) \rightarrow 3s^23p^43d(^4F_{5/2})$	1.84E+6	1.692E+6 ^[17]
1	12	543	$3s^23p^5(^2P_{3/2}^o) \rightarrow 3s^23p^43d(^2P_{1/2})$	9.696E+6 9.57E+6	7.889E+6 ^[17]
2	12	459.5	$3s^23p^5(^2P_{1/2}^o) \rightarrow 3s^23p^43d(^2P_{1/2})$	3.930E+7 3.87E+7	3.503E+7 ^[17]
1	14	440	$3s^23p^5(^2P_{3/2}^o) \rightarrow 3s^23p^43d(^4P_{1/2})$	1.350E+7 1.31E+7	1.243E+7 ^[17]
1	15	439	$3s^23p^5(^2P_{3/2}^o) \rightarrow 3s^23p^43d(^4P_{3/2})$	3.90E+6 3.77E+6	5.367E+6 ^[17]
1	16	437.3	$3s^23p^5(^2P_{3/2}^o) \rightarrow 3s^23p^43d(^4P_{5/2})$	2.740E+6 2.66E+6	2.754E+6 ^[17]
1	17	437.8	$3s^23p^5(^2P_{3/2}^o) \rightarrow 3s^23p^43d(^2D_{3/2})$	6.530E+7 6.45E+7	5.201E+7 ^[17]
1	18	434.6	$3s^23p^5(^2P_{3/2}^o) \rightarrow 3s^23p^43d(^2D_{5/2})$	1.920E+8 1.90E+8	1.576E+8 ^[17]
1	27	341.3	$3s^23p^5(^2P_{3/2}^o) \rightarrow 3s^23p^43d(^2S_{1/2})$	6.23E+10 6.43E+10	4.264E+10 ^[17] ,6.543E+10 ^[17]

transitions (E2,E3,M1,M2) have longer lifetimes than those through dipole allowed transitions (same spin E1d and intercombination E1i). No lifetimes for Ca IV levels were found in literature for comparison. However, their accuracies are related to those of the A-values which have been discussed for Table 4.

5 Conclusion

We have studied collision strength of Ca IV using a 54-levels close coupling wave function expansion that corresponds to target ion excitations to high lying levels. This ensures inclusion of converged contributions of resonances generated by all the levels. We have demonstrated the effect of number of partial waves in the collision strength Ω and showed convergence of partial waves contributing to collision strengths.

Features of Ω show resonances in the low energy region but they converge to the background much before reaching the highest 54th excitation of Ca IV. We find that Ω of the emission line of 3.2 μm due to collisional excitation of $^2P_{3/2}^o - ^2P_{1/2}^o$ of ground configuration $3s^23p^5$ has extensive resonances with

Table 5 Lifetimes of a few levels illustrating the complete table of lifetimes of all 386 levels. Radiative decay rates of level j to various lower levels $j \rightarrow i$ are given. Notation C is for configuration, g for statistical weight factor, lv for level, f for f-value for an E1 transition or S-values for E2, E3, M1, M2 transitions, A for A-value and E for transition energy.

Type	LSi	Ci	gi	lvi	LSj	Ci	gj	lvj	f(E1)/S(E2, E3,M1,M2)	Aji (s ⁻¹)	Eij (Å)
lifetime: sslevel j= 2, Cf= 1, ² P _{1/2} ^o [E= 3.019E-02 Ry= 3.3134852E+03 /cm]											
E2	² P ^o	1	4	1	² P ^o	1	2	2	1.54E+00	5.180E-05	3.0180E+04
M1	² P ^o	1	4	1	² P ^o	1	2	2	1.33E+00	6.540E-01	3.0180E+04
Summed A-values: Af (forbidden)= 6.541E-01, Aa (allowed)= 0.000E+00 s-1											
Total Sum(Af+Aa)= Aji (2 transitions) to the level= 6.541E-01 s-1											
Lifetime (=1/Aji)= 1.529E+00 s											
lifetime: sslevel j= 7, cf= 3, ⁴ D _{1/2} [E= 1.826E+00 Ry= 2.0041544E+05 /cm]											
E1i	² P ^o	1	4	1	⁴ D	3	2	7	1.01E-06	5.420E+04	4.9896E+02
E1i	² P ^o	1	2	2	⁴ D	3	2	7	3.96E-06	1.030E+05	5.0735E+02
E2	² S	2	2	3	⁴ D	3	2	7	0.00E+00	0.000E+00	1.7417E+03
M1	² S	2	2	3	⁴ D	3	2	7	3.18E-07	8.120E-04	1.7417E+03
E2	⁴ D	3	6	5	⁴ D	3	2	7	1.15E-03	2.890E-12	2.0196E+05
E2	⁴ D	3	6	5	⁴ D	3	2	7	1.15E-03	2.890E-12	2.0196E+05
E2	⁴ D	3	4	6	⁴ D	3	2	7	2.69E-03	1.120E-13	4.5789E+05
M1	⁴ D	3	4	6	⁴ D	3	2	7	5.97E+00	8.380E-04	4.5789E+05
Summed A-values: Af (forbidden)= 1.650E-03, Aa (allowed)= 1.572E+05 s-1											
Total Sum(Af+Aa)= Aji(8 transitions) to the level= 1.572E+05 s-1											
Lifetime (=1/Aji)= 6.361E-06 s											

enhanced background in the low energy region. This has resulted in a strong effective collision strength Υ with a peak around 3×10^5 K indicating a distinct presence of an emission line when the environmental plasma effects are low. The 3.2 μm line is within the wavelength range of JWST.

The present Ω has shown expected features at high electron energy, such as, decaying background for the forbidden transitions, slow decay or almost constant value for weak dipole transitions and rising trend of Coulomb Bethe $\ln(E)$ behavior toward a plateau for strong dipole allowed transitions.

We present a set of over 93,000 radiative transitions among 387 energy levels with orbitals going up to 5s in Ca IV. Results include lifetimes of all 386 excited levels.

The present results are expected to be accurate and large enough for the two processes to provide a complete astrophysical modeling for all practical purposes.

Data availability. All atomic data for energies, radiative transitions, collisional excitations, and effective collision strengths of a set of transition are available online at the NORAD-Atomic-Data database at the Ohio State University at: <https://norad.astronomy.osu.edu/>

Acknowledgments. All computations were carried on the high performance computers of the Ohio Supercomputer Center. BS acknowledges of IRSIP fellowship from the Government of Pakistan to carry out the research at the Ohio State University.

Declarations

Both authors, S.N. Nahar and B. Shafique, contributed equally on the contents of the paper. While SNN trained BS, set up the project, wrote necessary program, and remained engaged in studying the project, BS picked up all aspects of computations, carried out computations, and was engaged in the analysis.

References

- [1] Shore SN, Augusteijn T, Ederoclite A, and Uthas H 2011 *A&A* **533** L8
- [2] Asplund M, Grevesse N, Sauval AJ, and Scott P, 2009 *Annu. Rev. Astron. Astrophys.* **47**, 481–52
- [3] Shepherd J 2019, <https://www.astrobin.com/full/406485/0/>
- [4] Jacobson-Galan W V et al, 2020, *Astrophys. J.* **898** 166
- [5] Feuchtgruber H et al 1997 *ApJ* **487** 962
- [6] Ignanc R, Cassinelli JP, Quigley M, Babler B 2001 *ApJ* **558** 771-779
- [7] Feuchtgruber H, Lutz D, Beintema D A 2001 *ApJS* **136** 221
- [8] Zuckerman B, Koester D, Reid I N, and Hunsch M 2003 *ApJ* **596** 477
- [9] Pradhan A K and Nahar S N 2011 *Atomic Astrophysics and Spectroscopy* (Cambridge University press, New York)
- [10] Sugar J and Corliss C 1985 *J. Phys. Chem. Ref. Data* **14**, Suppl. **2** 1-664
- [11] https://physics.nist.gov/PhysRefData/ASD/levels_form.html
- [12] Naqvi A M 1951 *PhD Thesis Harvard University* 192pp (data available at NIST)
- [13] Varsavsky C M 1961 *Astrophys. J., Suppl. Ser.* **6** 75-107
- [14] Fawcett B C and Gabriel A H 1966 *Proc. Phys. Soc.* **88** 262
- [15] Gabriel A H, Fawcett B C, Jordan C 1966 *Proc. Phys. Soc.* **87** 825
- [16] Huang K -N, Kim Y -K, Cheng K T and Desclaux J P 1983 *ADNDT* **28** 355-377
- [17] Wilson N J, Hibbert A and Bell K L, 2000 *Phys.Scr.* **61** 603-610

- [18] Hummer D G, Berrington K A, Eissner W, Pradhan A K, Saraph H E, and Tully J A 1993 *Astron Astrophys* **279** 298-309
- [19] Berrington K A, Eissner W, and Norrington P H 1995 *Comput Phys Commun* **92** 290-420
- [20] Eissner W, Jones M and Nussbaumer H 1974 *Comput. Phys. Commun.* **8**, 270-306
- [21] Nahar S N, Eissner W, Chen G X and Pradhan A K 2003 *A&A* **408** 789
- [22] Burgess A and Tully JA 1978 *J. Phys. B* **11** 4271
- [23] Burke P G and Robb W D 1975 *Adv. At. Mol. Phys.* **11** 143-214
- [24] Scott N S and Burke P G 1980 *J. Phys. B* **12** 4299
- [25] Scott N S and Taylor K T 1982 *Comput. Phys. Commun.* **25** 347
- [26] Nahar S N, written in 2013, unpublished
- [27] NORAD-Atomic-Data: <https://norad.astronomy.osu.edu/>